Int. J. Electrochem. Sci., 14 **(2019)** 7643 – 7651, doi: 10.20964/2019.08.39

International Journal of
ELECTROCHEMICAL
SCIENCE
www.electrochemsci.org

The Electrochemical Performance of Mg-F Co-doped Spinel $LiNi_{0.5}Mn_{1.5}O_4$ Cathode Materials for Lithium-Ion Battery

Chao Ma[1,*], *Le Luo*[1], *Kewei Li*[1], *Bo Zhou*[1], *Qin Shi*[2,*]

[1] Scool of Electronic Engineering, Chengdu Technological University, Chengdu 611730, China
[2] Department of Physics, Shihezi University, Shihezi 832003, China
[*]E-mail: chaoma@yahoo.com, aistarsq@sina.com

Received: 6 April 2019 / *Accepted:* 23 May 2019 / *Published:* 30 June 2019

The Mg doped and Mg-F co-doped spinel $LiNi_{0.5}Mn_{1.5}O_4$ nanoparticles have been synthesized using a rheological method and investigated as high voltage cathode materials for rechargeable lithium-ion batteries. The results demonstrate that the Mg-F co-doped $LiNi_{0.5}Mg_{0.2}Mn_{1.3}O_{3.8}F_{0.4}$ cathodes present an improved electrochemical performance over the pristine and Mg doped samples. After cycling at different current densities at 55 °C, the discharge capacities are 101.4 mAh g^{-1} for the $LiNi_{0.5}Mg_{0.2}Mn_{1.3}O_{3.8}F_{0.4}$ cathode (90 % of the capacity retention), 73.3 mAh g^{-1} for the $LiNi_{0.5}Mg_{0.2}Mn_{1.3}O_4$ sample (71 % of the capacity retention), and 43.1 mAh g^{-1} for the pristine $LiNi_{0.5}Mn_{1.5}O_4$ material (49 % of the capacity retention). The remarkable performances may be attributed to the doping of Mg ions which in turn suppress the John-Teller effect by increasing the average oxidation state of Mn ions. Furthermore, the doping of F ions provide a more stable crystal structures and smaller charge transfer resistance.

Keywords: Lithium-ion battery, Cathode material, Co-doping, Rate capability, High temperature

1. INTRODUCTION

Owing to the requirements of the global low-carbon society and the rapid depletion of fossil fuels, the rechargeable lithium-ion batteries (LIBs) are regarded as one of the high efficiency low cost, and environmentally friendly electrochemical energy conversion and storage devices [1]. In recent years, the LIB has been recognized as a potential candidate for replacing fossil fuels in vehicular applications [2]. The worldwide demand of the applications in electric vehicles (EVs) or hybrid EVs (HEVs) not only greatly stimulate the development of LIBs, but also result in a higher expectation on designing electrodes with high energy and power density [3]. As the performance of the high energy and power in rechargeable LIBs strongly depend on the properties of their materials, considerable attention has been

paid to the research and development of high voltage cathode materials [4]. Recently, the manganese site doped spinel $LiNi_{0.5}Mn_{1.5}O_4$ material has attracted a great deal of interest for the application of cathode materials for lithium ion batteries due to the existence of its high-voltage plateau and high value of theoretical energy density (691 Wh kg^{-1}=147 mAh g^{-1}×4.7 V) [5, 6]. Despite such advantages, significant capacity decay during cycling, especially at elevated temperature, has hindered the commercialization of $LiNi_{0.5}Mn_{1.5}O_4$ as a cathode material for LIBs [7].

Several possible mechanisms for the degradation in electrochemical performances have been suggested, such as: dissolution of Mn^{2+} that originates from the disproportionation reaction of Mn^{3+} [8], John-Teller distortion on the crystal structure at the end of discharge, i.e. large change in the unit cell volume due to loss of Mn^{3+} ions [9], and lattice instability due to structural changes during the cycling process where Li is inserted and extracted [1]. In order to improve the cycling performance in $LiNi_{0.5}Mn_{1.5}O_4$ cathode material, it is essential to minimize the influence of Mn^{3+} ions as well as improving the stability of the crystallite structures [10]. In this work, the cation and anion co-doped $LiNi_{0.5}Mg_yMn_{1.5-y}O_{4-y}F_{2y}$ material was synthesized. The analysis and comparison of their crystal structure, morphology, and electrochemical properties of the Mg-F co-doped, Mg doped, and pristine $LiNi_{0.5}Mn_{1.5}O_4$ cathode materials were addressed. The mechanisms of cation and anion co-doping to improve the performance of $LiNi_{0.5}Mn_{1.5}O_4$ cathode materials were also discussed.

2. EXPERIMENTAL

$LiNi_{0.5}Mg_xMn_{1.5-x}O_4$ (x = 0, 0.1 and 0.2) and $LiNi_{0.5}Mg_yMn_{1.5-y}O_{4-y}F_{2y}$ (y = 0.1 and 0.2) powders were synthesized through the rheological method and the samples were labeled as S0, S1, S2, S11 and S22, respectively. Analytical grade $Li(CH_3COO)\cdot 2H_2O$, $Ni(CH_3COO)_2\cdot 4H_2O$, $Mg(CH_3COO)_2\cdot 4H_2O$, $Mn(CH_3COO)_2\cdot 4H_2O$ and LiF were used as raw materials according to the cation stoichiometric ratio. The specific method was described in the literature [11].

The phase structure analysis and sample crystallization were investigated by X-ray diffraction (XRD, Bruker D8). The morphology of the particles was characterized by scanning electron microscopy (SEM, Supra55VP, Zeiss).

Electrode laminates were made by casting a slurry of 80 wt % active oxide, 10 wt % acetylene black and 10 wt % polyvinylidene fluoride (PVDF) in 1-methy-1-pyrrolidinone solvent onto an Al foil. The cast laminates were dried in vacuum at 100 °C for 10 h and punched into circular pieces having a diameter of 1 cm. The Lithium coin cells were assembled using the as-prepared cathode, a lithium metal foil as counter electrode and a porous polypropylene film (Celgard 2400) as a separator. The electrolyte was 1 M $LiPF_6$ in 1:1 EC/DMC. Lithium coin cells (CR2025) were carried out in an Ar-filled glovebox.

Charge/discharge tests were performed on a multi-channel battery test system (BTS-51, Neware, China) at room temperature and 55 °C, respectively, between a voltage range of 3.5 and 4.9 V and with the current density ranging from 0.2 to 5 C rate (assuming the theoretical capacity of 150 mAh g^{-1}). Electrochemical impedance spectroscopy (EIS) was measured on an electrochemical workstation (CHI650C, Shanghai, China) by applying an AC signal in the frequency range between 10^{-2} - 10^5 Hz with a voltage 5 mV_{P-P} after charging the cells up to a potential of 4.9 V.

3. RESULTS AND DISCUSSION

The XRD patterns of the powder samples are shown in Fig.1. All samples have been identified as polycrystalline structures with cubic spinel phases (according to JCPDS-ICDD 80-2162， space group $Fd\bar{3}m$). From the presence of several peaks, it can be concluded that Mg and F ions have fully doped in the $LiNi_{0.5}Mn_{1.5}O_4$ compounds. The strong and narrow diffraction peaks suggest that the well-crystallized powder samples have formed successfully. No other peak related to a secondary phase is identified in S11 and S22, which means that the lattice structures have not undergone any change post the doping of Mg and F and form a solid solution. However, the impurity phases of NiO are detected from the small peaks at about $2\theta = 43.8°$ in pristine and Mg doped samples. This is consistent with the previous findings [11]. It is noted that the space group $Fd\bar{3}m$ means the disordered spinel structure and the chemical formula should be written as $LiNi_{0.5}Mn_{1.5}O_{4-\delta}$. It is more conducive to the diffusion of lithium ions compared the ordered spinel structure which has the space group of $P4_332$ [12].

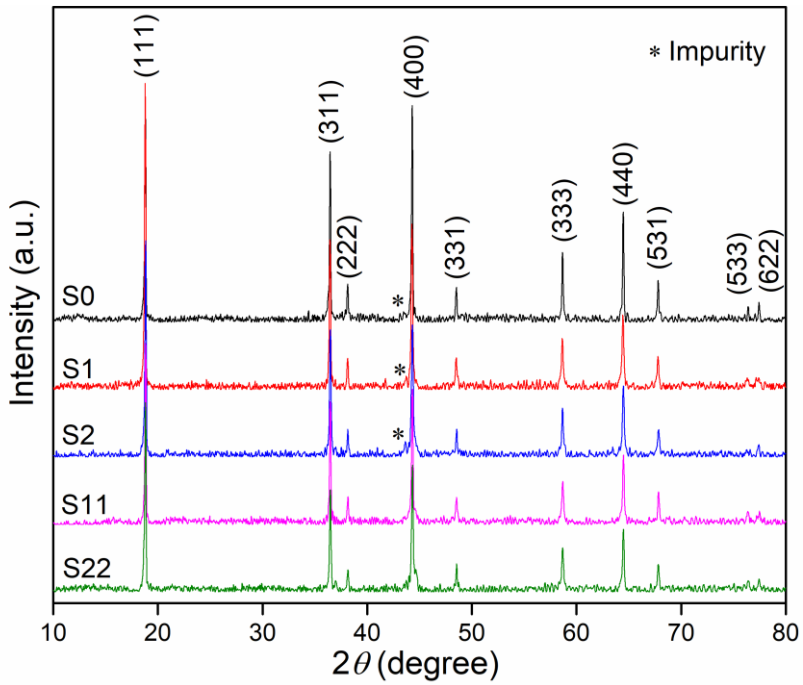

Figure 1. XRD patterns of samples prepared through the rheological method.

The calculated lattice constants are shown in Tab. 1. The data provides significant information regarding the structural evolution of the doped samples. Compared with sample S0, the lattices of doped samples are expanded in dimension with increased content of the dopants. Since the radius of Mg^{2+} (0.72 Å) is much larger than Mn^{4+} (0.53 Å), the lattice constants of S22 and S11 samples are larger than S2 and S1, respectively. Even though the radius of F^- is smaller than O^{2-}. Some researchers indicated that the difference in the ionic size of Mg^{2+} and Mn^{4+} may enhance the lattice disorder on the spinel $LiNi_{0.5}Mn_{1.5}O_4$ solid solutions [13]. Besides, the loss of O ions can also lead to the enhancement in the disorder of the spinel structure [14].

Table 1. Lattice constants of powdered samples. Numbers in brackets denote the standard deviations.

Sample	a (Å)
S0	8.1669 (0.0005)
S1	8.1673 (0.0004)
S2	8.1681 (0.0003)
S11	8.1674 (0.0006)
S22	8.1682 (0.0005)

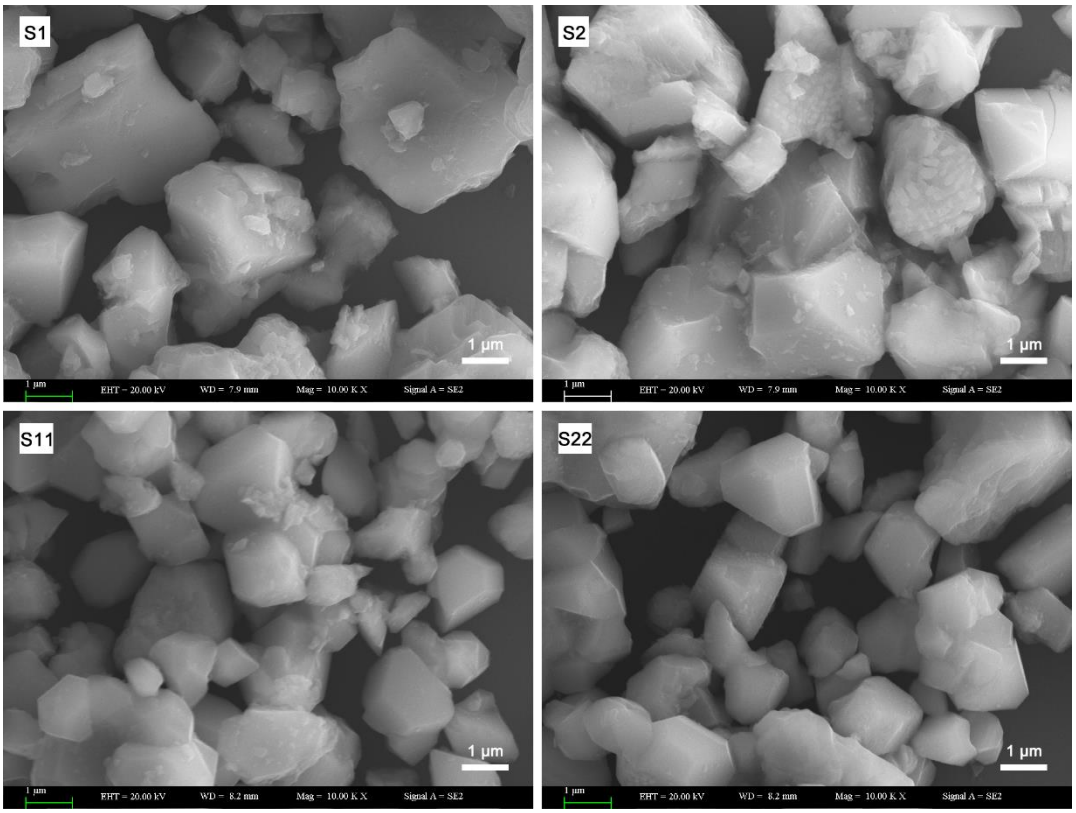

Figure 2. SEM images of doped powder samples.

The SEM images of $LiNi_{0.5}Mg_xMn_{1.5-x}O_4$ and $LiNi_{0.5}Mg_yMn_{1.5-y}O_{4-y}F_{2y}$ particles are shown in Fig. 2. All the samples have a dense polyhedron shape with a smooth surface. The particle size of the samples is mainly distributed in the range between 2 - 3 µm. Moreover, the particles of the samples are distributed uniformly. Large sized uniform particle distribution always has a smaller surface area, which can reduce the area of contact between the cathode and the electrolyte, and further reduce the corrosion of the active materials by the electrolyte [15]. The observations of morphology indicate that the doping of a small amount of Mg and F ions do not significantly affect the size of the materials. From this point of view, the effect of particle size on the electrochemical properties of the samples can be considered to be mainly attributed to the Mg and F substitution rather than the morphology or the grain size.

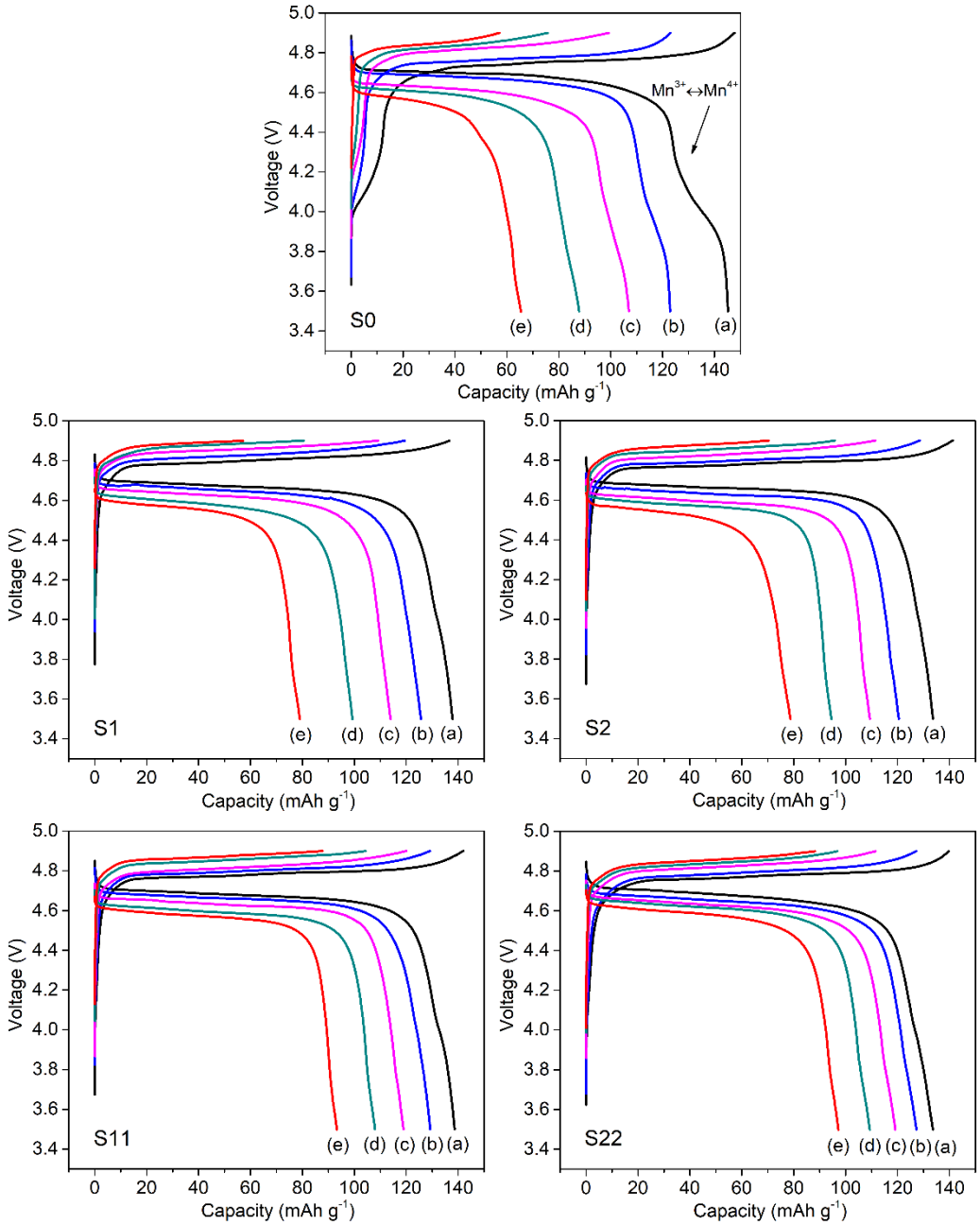

Figure 3. Charge-discharge profiles of the spinel Li//$LiNi_{0.5}Mg_xMn_{1.5-x}O_4$ (S0, S1 and S2) and Li//$LiNi_{0.5}Mg_yMn_{1.5-y}O_{4-y}F_{2y}$ (S11 and S22) cells in the voltage range of 3.5 to 4.9 V at (a) 0.2 C, (b) 0.5 C, (c) 1 C, (d) 2 C and (e) 5 C rates.

The charge-discharge curves for the $LiNi_{0.5}Mg_xMn_{1.5-x}O_4$ (x=0, 0.1 and 0.2) and $LiNi_{0.5}Mg_yMn_{1.5-y}O_{4-y}F_{2y}$ (y=0.1 and 0.2) cathode materials were carried out at room temperature between 3.5 to 4.9 V, at 0.2 C, 0.5 C, 1 C, 2 C and 5 C. The results are shown in Fig. 3. In all cases, the voltage plateau is present at around 4.7 V, reflecting the Ni^{2+}/N^{4+} redox reaction [16]. The other plateau located at around 4.1 V can be related to the redox reaction of Mn^{3+}/Mn^{4+} [17]. It can be found that the initial discharge curve of $LiNi_{0.5}Mn_{1.5}O_4$ presents an obvious plateau in the potential region around 4.1 V, which is almost invisible in doped materials. We can conclude that the Mg^{2+} ions may suppress the

lower valance states of the Mn ions during cycling to maintain a chemical equilibrium. As we know, Mn^{3+} can induce a Jahn-Teller structural distortion and dissolve into the electrolyte via a disproportionation reaction, which however, has an adverse effect on the capacity retention [7, 9]. Therefore, the doped samples have better performances especially at high current rates. At the same time, the initial discharge capacities are decreased with increasing Mg contents. This result is consistent with the previous studies, that the doping would lead to a decreased specific charge [18]. In addition, S1 and S11 samples have almost the same capacities during the initial cycling, while the sample S1 results in larger capacity decay during high rate cycling. The relationship between the S2 and S22 samples is consistent with the measurement framework of S1 and S11. As mentioned before, the S2 and S22 samples have the smaller initial discharge capacities, but they have better performance at a high cycling rate, especially for the S22 sample. Previous investigations indicated that the cycling and rate performances of the disordered spinel structure are superior to that of the ordered one owing to the higher Li^+ diffusion coefficients [7]. It is confirmed by the XRD data that the structural disorder can be enhanced with the increase of dopants in a spinel lattice. Therefore, we can attribute the improvements in the performances of cathode materials to the Mn-F co-doping.

To further explore the reasons of the improved performances of the doped materials, we carried out the charge-discharge cyclic performance tests at a high temperature in the constant temperature and humidity environmental chamber.

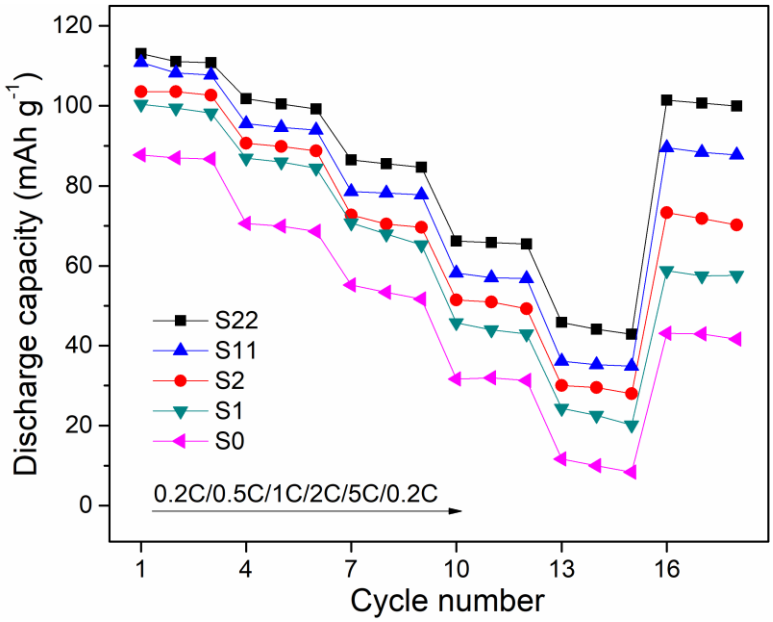

Figure 4. Discharge capacities of the pristine and the doped cathode materials at different current rates under 55 °C.

Fig. 4 shows the discharge capacities of the pristine and doped electrodes at different rates, measured at 55 °C. The procedure consists of applying 0.2, 0.5, 1, 2 and 5 C rates thrice for

charge/discharge cycles followed by the final measurement at 0.2 C rate. It is seen that with the current density increasing gradually, the discharge capacities of all the samples are rapidly reduced. It is obviously seen that the rate performance of Mg-F co-doped samples is more stable than that of Mg-doped and pristine samples, and the rate performance is getting better with the increase of the co-doping content. The initial discharge capacities are 87.7, 100.4, 103.6, 110.9 and 113.1 mAh g^{-1} at 0.2 C rate, and the capacity retentions are 49 %, 59 %, 71 %, 81 % and 90 % after different rate cycling for S0, S1, S2, S11 and S22 samples, respectively. Some other studies also proved that the doping was a useful method to improve the electrochemical properties of the $LiNi_{0.5}Mn_{1.5}O_4$. Upon running for 40 cycles at room temperature, the $LiNi_{0.4}Cr_{0.15}Mn_{1.45}O_4$ electrode delivered a reversible discharge capacity of 139.7 mAh g^{-1} with a capacity retention of 97.08%. In contrast, the $LiNi_{0.5}Mn_{1.5}O_4$ only maintains a reversible discharge capacity of 127.7 mAh g^{-1} with a capacity retention of 93.48 % [19].

In this study, the magnitude relationships of the initial discharge capacity values, measured under 55 °C (S22 > S11 > S2 > S1) are different from ones measured at room temperature. The reaction of the electrolytes and the electrode materials is more intense at a higher measurement temperature. More Mg contents mean less Mn^{3+}, thus reducing the dissolution of the Mn ions and enhancing the stability of the spinel structure while performing the cycling tests. Therefore, the discharge capacities are increased with increasing Mg contents. On the other hand, due to the very high ionicity of the metal-fluorine chemical bond, the introduction of the F ions can stabilize the cubic structure of the spinel upon performing repeated electrochemical cycles [8, 19]. This is believed to be the main reason for the improvement of the rate performance in F^- doped materials at high measurement temperature. In addition, the previous work indicated that the addition of F^- would expand the diffusion pathway of Li^+ and the depth of Li^+ intercalation and deintercalation could be increased by enhancing the intrinsic electronic conductivity and resulting the good rate capability at high rate and high temperature [20]. With this view in mind, the EIS is employed to analyze the impedance of the electrodes.

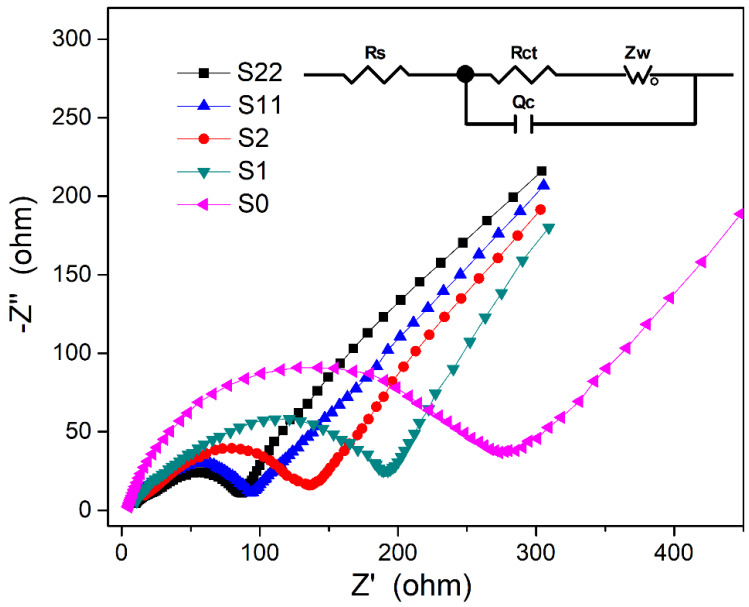

Figure 5. The Nyquist spectra of the pristine and the doped cathode materials.

Fig. 5 depicts the Nyquist plots of the pristine and the doped samples. The Nyquist plots of all the samples consist of a semicircle in the high-to-medium frequency region associated with the charge transfer resistance (R_{ct}). A sloping line at the low frequency range corresponding to the Warburg impedance that is associated with Li^+ diffusion in the electrodes [15]. An equivalent circuit describing the Randles model is used for fitting the experimental data (inset of Fig. 5), where R_s is the ohmic resistance, R_{ct} is the charge transfer resistance of the electrodes, Z_w is the Warburg impedance and Q_c is the constant phase element [9]. The fitting results are shown in Tab. 2. As seen from the Nyquist plots and fitted data, it can be found that although the radius of the semicircle of S22 is smaller than that of the S11 electrode, the apparent difference of R_{ct} is not observed. However, the radii of the semicircles in the Mg-F co-doped electrodes are much smaller than that of the pristine and Mg-doped samples, indicating that a much smaller charge transfer resistances is recorded for the Mg-F co-doped electrodes. The experimental spectra fitted well with the calculated values. This is strong evidence that the F^- doped samples possess a superior conductivity [21]. Previous study showed that the charge-transfer resistance of the Mo doped $LiNi_{0.5}Mn_{1.5}O_4$ is much smaller than that of the pristine $LiNi_{0.5}Mn_{1.5}O_4$, indicating that the active materials with a large electronic conductivity and high rate capability can be obtained by doping [22].

Table 2. Impedance parameters obtained from equivalent circuit fitting of experimental data for the pristine and the doped cathode materials.

Sample	R_s (Ω)	R_{ct} (Ω)
S0	16.9	286.9
S1	13.7	229.5
S2	11.2	159.2
S11	6.6	102.4
S22	6.4	96.7

4. CONCLUSIONS

In summary, Mg doped $LiNi_{0.5}Mg_xMn_{1.5-x}O_4$ and Mg-F co-doped $LiNi_{0.5}Mg_yMn_{1.5-y}O_{4-y}F_{2y}$ cathode materials used for fabricating lithium ion batteries are synthesized successfully via a rheological method. The co-doped $LiNi_{0.5}Mg_{0.2}Mn_{1.3}O_{3.8}F_{0.4}$ sample exhibits excellent electrochemical performances at high temperatures, such as high cycling stability and rate capability. The improved electrochemical properties can be attributed to the synergetic effects of the incorporation of the Mg and F ions. Mg-doping can reduce the content of Mn^{3+} during the cycling that may not only suppress the Jahn-Teller effect but also prevent the dissolution of the electrodes. While the F-doping is regarded for increasing the bond strength with metal ions, and this in turn facilitates the charge transfer among the electrode materials. The outstanding electrochemical performance would make the Mg-F co-doped $LiNi_{0.5}Mg_yMn_{1.5-y}O_{4-y}F_{2y}$ material a promising LIB cathode material through continuous refining.

ACKNOWLEDGEMENTS
This work was supported by the Research Project of the Introduction Talent (No. 2017RC015).

References

1. Y. G. Guo, J. S. Hu, L. J. Wan, *Adv. Mater.*, 20 (2008) 2878.
2. S. R. Gowda, V. Pushparaj, S. Herle, G. Girishkumar, J. G. Gordon, H. Gullapalli, X. Zhan, P. M. Ajayan, A. L. Reddy, *Nano. Lett.*, 12 (2012) 6060.
3. R. Ramachandran, S. M. Chen, *Int. J. Electrochem. Sci.*, 10 (2015) 9488.
4. J. B. Goodenough, Y. Kim, *Chem. Mater.*, 22 (2010) 587.
5. D. Aurbach, B. Markovsky, Y. Talyossef, G. Salitra, H. J. Kim, S. Choi, *J. Power Sources*, 162 (2006) 780.
6. N. Mokhtar, N. H. Idris, M. F. M. Din, *Int. J. Electrochem. Sci.*, 13 (2018) 10113.
7. J. Yang, X. Han, X. Zhang, F. Cheng, J. Chen, *Nano Res.*, 6 (2013) 679.
8. Y. Abu-Lebdeh, I. Davidson, Nanotechnology for Lithium-Ion Batteries, Springer US, (2013) New York, US.
9. G. P. Nayaka, J. Manjanna, K. C. Anjaneya, P. Manikandan, P. Periasamy, V. S. Tripathi, *Bull. Mat. Sci.*, 37 (2014) 705.
10. C. C. Pan, C. E. Banks, W. X. Song, C. W. Wang, Q. Y. Chen, X. B. Ji, *Trans. Nonferrous Met. Soc. China*, 23 (2013) 108.
11. C. Ma, L. Wang, H. Yang, H. Liu, *Int. J. Electrochem. Sci.*, 13 (2018) 8170.
12. J. H. Kim, S. T. Myung, C. S. Yoon, S. G. Kang, Y. K. Sun, *Chem. Mat.*, 16 (2004) 906.
13. G. P. Nayaka, K. V. Pai, J. Manjanna, K. C. Anjaneya, P. Periasamy, V. S. Tripathi, *Bull. Mat. Sci.*, 39 (2016) 1279.
14. J. Cabana, M. Casas-Cabanas, F. O. Omenya, N. A. Chernova, D. Zeng, M. S. Whittingham, C. P. Grey, *Chem. Mater.*, 24 (2012) 2952.
15. J. Dou, X. Kang, T. Wumaier, H. Yu, N. Hua, Y. Han, G. Xu, *J. Solid State Electrochem.*, 16 (2011) 1481.
16. C. Locati, U. Lafont, L. Simonin, F. Ooms, E. M. Kelder, *J. Power Sources*, 174 (2007) 847.
17. F. U. Okudur, J. D'Haen, T. Vranken, D. De Sloovere, M. Verheijen, O. M. Karakulina, A. M. Abakumov, J. Hadermann, M. K. Van Bael, A. Hardy, *RSC Adv.*, 8 (2018) 7287.
18. N. Amdouni, K. Zaghib, F. Gendron, A. Mauger, C. M. Julien, *Ionics*, 12 (2006) 117.
19. S. Wang, P. Li, L. Shao, K. Wu, X. Lin, M. Shui, N. Long, D. Wang, J. Shu, *Ceram. Int.*, 41 (2015) 1347.
20. L. Yang, L. Jiao, Y. Miao, H. Yuan, *J. Solid State Electrochem.*, 14 (2009) 1001.
21. D. Wang, K. Zhang, L. Liao, S. Chen, A. Qin, *Int. J. Electrochem. Sci.*, 14 (2019) 102.
22. T. F. Yi, B. Chen, Y. R. Zhu, X. Y. Li, R. S. Zhu, *J. Power Sources*, 247 (2014) 778.

© 2019 The Authors. Published by ESG (www.electrochemsci.org). This article is an open access article distributed under the terms and conditions of the Creative Commons Attribution license (http://creativecommons.org/licenses/by/4.0/).